The perturbation pressure, p', can be represented as the sum of a hydrostatic pressure perturbation p'_{h} and a nonhydrostatic pressure perturbation p'_{nh}, that is,

$$p' = p'_{\mathrm{h}} + p'_{\mathrm{nh}}. \tag{2.122}$$

The former arises from density perturbations by way of the relation

$$\frac{\partial p'_{\mathrm{h}}}{\partial z} = -\rho' g, \tag{2.123}$$

which allows us to rewrite the inviscid form of (2.56) as

$$\frac{\mathrm{d}w}{\mathrm{d}t} = -\frac{1}{\rho}\frac{\partial p'_{\mathrm{nh}}}{\partial z}. \tag{2.124}$$

Hydrostatic pressure perturbations occur beneath buoyant updrafts (where $p'_{\mathrm{h}} < 0$) and within the latently cooled precipitation regions of convective storms (where $p'_{\mathrm{h}} > 0$) (e.g., Figure 5.23). The nonhydrostatic pressure perturbation is simply the difference between the total pressure perturbation and hydrostatic pressure perturbation and is responsible for vertical accelerations. An alternate breakdown of pressure perturbations is provided below.

$$\frac{\mathrm{d}w}{\mathrm{d}t} = -\frac{1}{\rho}\frac{\partial p'}{\partial z} - \frac{\rho'}{\rho}g \tag{2.75}$$

$$= -\frac{1}{\rho}\frac{\partial p'}{\partial z} + B \tag{2.76}$$

where $B\,(= -\frac{\rho'}{\rho}g)$ is the buoyancy and $-\frac{1}{\rho}\frac{\partial p'}{\partial z}$ is the vertical perturbation pressure gradient force. The vertical perturbation pressure gradient force arises from velocity gradients and density anomalies. A more thorough examination of

For well-behaved fields (i.e., $\nabla^2 p' \propto -p'$),

$$p' \propto \underbrace{\underbrace{e_{ij}^2}_{\text{splat}}\ \underbrace{-\frac{1}{2}|\boldsymbol{\omega}|^2}_{\text{spin}}}_{\text{dynamic pressure perturbation}} \qquad \underbrace{-\frac{\partial B}{\partial z}}_{\text{buoyancy pressure perturbation}} . \tag{2.133}$$

where

$$e_{ij}^2 = \frac{1}{4}\sum_{i=1}^{3}\sum_{j=1}^{3}\left(\frac{\partial u_i}{\partial x_j} + \frac{\partial u_j}{\partial x_i}\right)^2 \tag{2.132}$$

and $u_1 = u$, $u_2 = v$, $u_3 = w$, $x_1 = x$, $x_2 = y$, and $x_3 = z$. Deformation describes the degree to which a fluid element changes shape as a result of spatial variations in the velocity field (e.g., fluid elements can be stretched or sheared by velocity gradients).

We see that deformation is always associated with high perturbation pressure via the e_{ij}^2 term, sometimes known as the *splat* term.[11] Rotation (of any sense) is always associated with low pressure by way of the $|\boldsymbol{\omega}|^2$ term, sometimes referred to as the *spin* term. We know that, hydrostatically, warming in a column leads to pressure falls in the region below the warming. The $\partial B/\partial z$ or *buoyancy pressure* term partly accounts for such hydrostatic effects.

Examples of the pressure perturbation fields associated with a density current (Section 5.3.2) and a buoyant, moist updraft are presented in Figures 2.6 and 2.7. In the case of the density current (Figure 2.6), positive p'_{h} and p'_{b} are found within the cold anomaly, with the maxima at the ground. A discrete excess in total pressure is present at the leading edge of the density current. This high pressure is a consequence of $p'_{\mathrm{nh}} > 0$ and $p'_{\mathrm{d}} > 0$ and the fact that $\left(\frac{\partial u}{\partial x}\right)^2$ is large there. There is also a prominent area of $p' < 0$ (and $p'_{\mathrm{d}} < 0$) centered behind the leading edge of the density current, near the top of the density current, associated with the horizontal vorticity that has been generated baroclinically.

In the case of the moist, buoyant updraft (Figure 2.7), a region of $p'_{\mathrm{h}} < 0$ (and $p'_{\mathrm{nh}} > 0$) is located beneath the buoyant updraft. A region of $p'_{\mathrm{d}} > 0$ exists above (below) the maximum updraft where horizontal divergence (convergence) is strongest; $\left(\frac{\partial u}{\partial x}\right)^2$ is large in both regions. On the flanks of the updraft, $p'_{\mathrm{d}} < 0$ as a result of the horizontal vorticity that has been generated baroclinically by the horizontal buoyancy gradients. The total p' field opposes the upward-directed buoyancy force, in large part as a result of the p'_{b} field (i.e., the p' and p'_{b} fields are well-correlated).

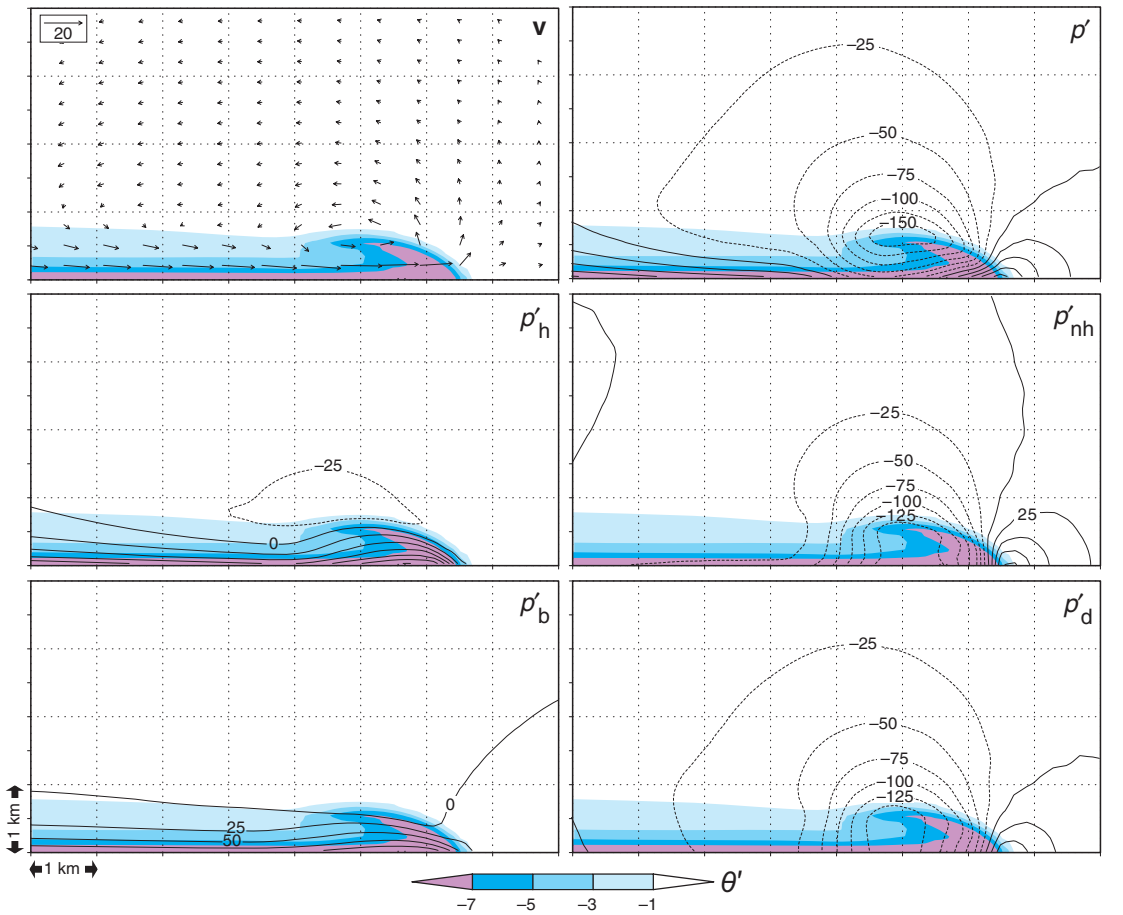

Figure 2.6 The pressure perturbations associated with a numerically simulated density current. The horizontal and vertical grid spacing of the simulation is 100 m. The ambient environment is unstratified. The domain shown is much smaller than the actual model domain used in the simulation. Potential temperature perturbations (θ') are shown in each panel (refer to the color scale). Wind velocity ($\mathbf{v}$) vectors in the x-z plane are shown in the top left panel (a reference vector is shown in the corner of this panel). Pressure perturbations are presented in the other panels. Units are Pa; the contour interval is 25 Pa = 0.25 mb (dashed contours are used for negative values). Note that $p' = p'_{\mathrm{h}} + p'_{\mathrm{nh}} = p'_{\mathrm{d}} + p'_{\mathrm{b}}$. The p'_{b} field was obtained by solving $\nabla^2 p'_{\mathrm{b}} = \frac{\partial(\overline{\rho}B)}{\partial z}$, where $\overline{\rho}$ is the base state density, using periodic lateral boundary conditions and assuming $\frac{\partial p'_{\mathrm{b}}}{\partial z} = 0$ at the top and bottom boundaries. (Regarding the boundary conditions, all that is known is that $\frac{\partial p'}{\partial z} = \overline{\rho}B$ at the top and bottom boundaries, owing to the fact that $\mathrm{d}w/\mathrm{d}t = 0$ at these boundaries, but it is somewhat arbitrary how one specifies the boundary conditions for $\frac{\partial p'_{\mathrm{b}}}{\partial z}$ and $\frac{\partial p'_{\mathrm{d}}}{\partial z}$ individually.) Because of the boundary conditions used, the retrieved p'_{b} field is not unique. A constant was added to the retrieved p'_{b} field so that the domain-averaged p'_{b} field is zero. The p'_{d} field was then obtained by subtracting p'_{b} from the total p' field.

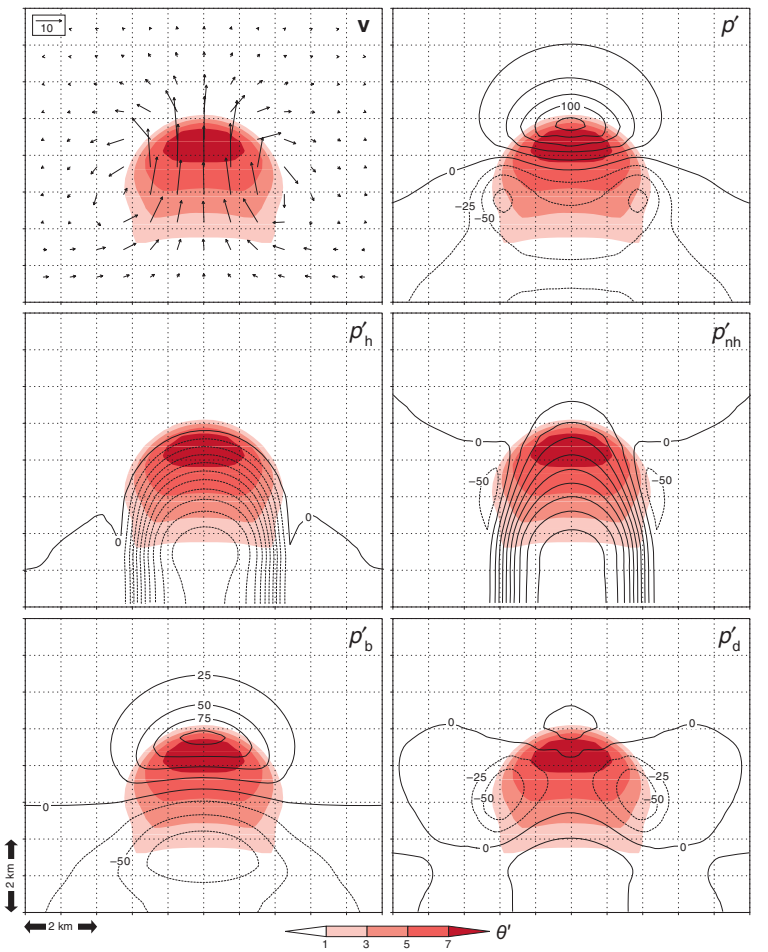

Figure 2.7 As in Figure 2.6, but for the case of a warm bubble released in a conditionally unstable environment. The bubble had an initial potential temperature perturbation of 2 K, a horizontal radius of 5 km, and a vertical radius of 1.5 km. The bubble was released 1.5 km above the ground. The fields shown above are from 600 s after the release of the bubble. The environment has approximately 2200 J kg^{-1} of CAPE and is the environment used in the simulations of Weisman and Klemp (1982). The horizontal and vertical grid spacing is 200 m (the domain shown above is much smaller than the actual model domain). The contour interval is 25 Pa (0.25 mb) for p', p'_b, and p'_d. The contour interval is 50 Pa (0.50 mb) for p'_h and p'_{nh}.

3.1.1 Vertical velocity of an updraft

If we multiply both sides of (3.1) by $w \equiv dz/dt$, we obtain

$$w\frac{dw}{dt} = B\frac{dz}{dt} \tag{3.11}$$

$$\frac{d}{dt}\left(\frac{w^2}{2}\right) = B\frac{dz}{dt} \tag{3.12}$$

Next, we integrate (3.12) over the time required to travel from the LFC to the equilibrium level (EL). We assume $w = 0$ at the LFC, since the only force considered here is the buoyancy force, which, by definition, does not become positive until the LFC is reached. Also, we assume that the maximum vertical velocity, w_{max}, occurs at the EL, which is consistent with the assumption that $dw/dt = B$ (neglecting the weight of hydrometeors in B). Integration of (3.12) yields

$$\int_{LFC}^{EL} dw^2 = 2\int_{LFC}^{EL} B\,dz \tag{3.13}$$

$$w_{EL}^2 - w_{LFC}^2 = 2\int_{LFC}^{EL} B\,dz \tag{3.14}$$

$$w_{max}^2 = 2\int_{LFC}^{EL} B\,dz \tag{3.15}$$

$$w_{max} = \sqrt{2\ \text{CAPE}}. \tag{3.16}$$

For CAPE $= 2000\ \text{J kg}^{-1}$, which corresponds to an average temperature (or virtual temperature) excess of $\approx$5 K over a depth of 12 km, parcel theory predicts $w_{max} = 63\ \text{m s}^{-1}$. The prediction of w_{max} in a convective updraft by (3.16) typically is too large, for several reasons discussed in the next section. Therefore, the value of w_{max} predicted by (3.16) can be interpreted as an upper limit for vertical velocity when buoyancy is the only force; w_{max} sometimes is called the *thermodynamic speed limit*.[4]

3.1.2 Limitations of parcel theory

Recall that we have neglected perturbation pressures in the preceding analysis of instability and maximum updraft velocity via (3.7) and (3.16), respectively (actually, we have neglected pressure perturbations *twice*—once in the vertical momentum equation, and once in the approximation for buoyancy). In general, the vertical perturbation pressure gradient is not negligible, and it tends to partially offset the acceleration induced by the buoyancy force.[5] As shown in Section 2.5.3, relatively high (low) pressure tends to be located above a warm (cold) bubble, and relatively low (high) pressure tends to be located beneath a warm (cold) bubble, causing a vertical gradient of the buoyancy pressure perturbation, p'_b (recall Figure 2.7). An *upward-directed* buoyancy force associated with a warm bubble tends to be associated with a *downward-directed* perturbation pressure gradient force, and a *downward-directed* buoyancy force associated with a cold bubble tends to be associated with an *upward-directed* perturbation pressure gradient force as dictated by (2.134).

A physical explanation for such perturbation pressures and their gradients is that a positive perturbation pressure (relatively high pressure) must exist above a rising bubble in order to push air laterally out of the way of the rising bubble, and a negative perturbation pressure (relatively low pressure) must exist beneath a rising bubble in order to draw air into the wake of the rising bubble and preserve mass continuity. Conversely, a cold bubble tends to have relatively high (low) pressure beneath (above) it for the same reasons. Furthermore, the presence of a temperature anomaly alone, regardless of whether or not it is rising or sinking, leads to pressure perturbations, owing to the fact that temperature anomalies are associated with thickness changes; that is, pressure surfaces are perturbed by temperature anomalies (thereby giving rise to pressure anomalies) in a hydrostatic atmosphere. In short, when considering the effect of the perturbation pressure gradient, isolated warm (cold) bubbles tend not to rise (sink) as fast as one would expect based on the consideration of the buoyancy force alone.

If the cold or warm anomaly is relatively narrow, then the buoyancy force is larger in magnitude than the perturbation pressure gradient forces, and warm (cold) air does in fact rise (sink). However, as a warm (cold) bubble increases in width, more air must be pushed out of its way in order for it to rise (sink), and more air must be drawn in below (above) to compensate for the wider region of ascent (descent). Thus, the opposing perturbation pressure gradient increases in magnitude with respect to the buoyancy force as a warm or cold bubble increases in width (Figure 3.1). When a warm or cold bubble becomes very wide, the opposing vertical perturbation pressure gradient becomes so large that it entirely offsets the buoyancy force, and the net acceleration is zero. This is the hydrostatic limit; in other words, the width scale of the temperature anomaly is very large compared with the depth scale, and the vertical pressure gradient and gravity are in balance. This is equivalent to setting $\nabla_h^2 p'_b = 0$ in (2.137), indicating a parcel of infinite horizontal extent, in which a case (2.137) reduces to

$$\alpha_0 \frac{\partial^2 p'_b}{\partial z^2} = -\frac{\partial}{\partial z}\left(\frac{\rho' g}{\rho_0}\right), \tag{3.17}$$

which can be simplified and integrated to yield

$$\frac{\partial p'_b}{\partial z} = -\rho' g, \tag{3.18}$$

in which case $p'_b = p'_h$, where p'_h is the hydrostatic pressure perturbation (recall Section 2.5.2). In this case, one could simply redefine the base state so that there are no density and pressure perturbations.

Parcel theory also neglects the exchange of momentum, moisture, and temperature between the parcel and its environment. Mixing of environmental air into a rising air parcel typically slows the parcel by reducing its buoyancy and upward momentum. This process is called *entrainment*. Entrainment can be viewed as a parcel dilution process, because the θ_e of a rising parcel typically is reduced by entrainment, leading to the realization of less CAPE and smaller w_{max} than predicted by (3.16) (Figure 3.2).

Updraft dilution increases with the tilt of an updraft, which increases the surface area of the updraft exposed to the hostile (subsaturated) environment. The entrainment into the sides of an updraft also increases as the vertical acceleration within the updraft increases, owing to mass continuity. It is possible to estimate the entrainment rate from *in situ* thermodynamic measurements within a cloud. As updraft width increases, the core of the updraft can become better shielded from the effects of entrainment. For this reason, skinny updrafts are more susceptible to the detrimental effects of entrainment than are wide updrafts. In simple one-dimensional cloud models, the entrainment rate is often parameterized in terms of updraft width. Updrafts are often wider in the presence of strong mesoscale ascent (e.g., ascent along an air mass boundary), which might be one reason why regions of mesoscale ascent are the most favorable locations for the initiation and maintenance of deep moist convection.

[5] An exception is for updrafts occurring in environments containing large vertical wind shear, in which the perturbation pressure gradient force may act in the same direction as buoyancy, especially at low levels, thereby augmenting the vertical acceleration. This effect will be discussed in greater detail in Chapter 8.

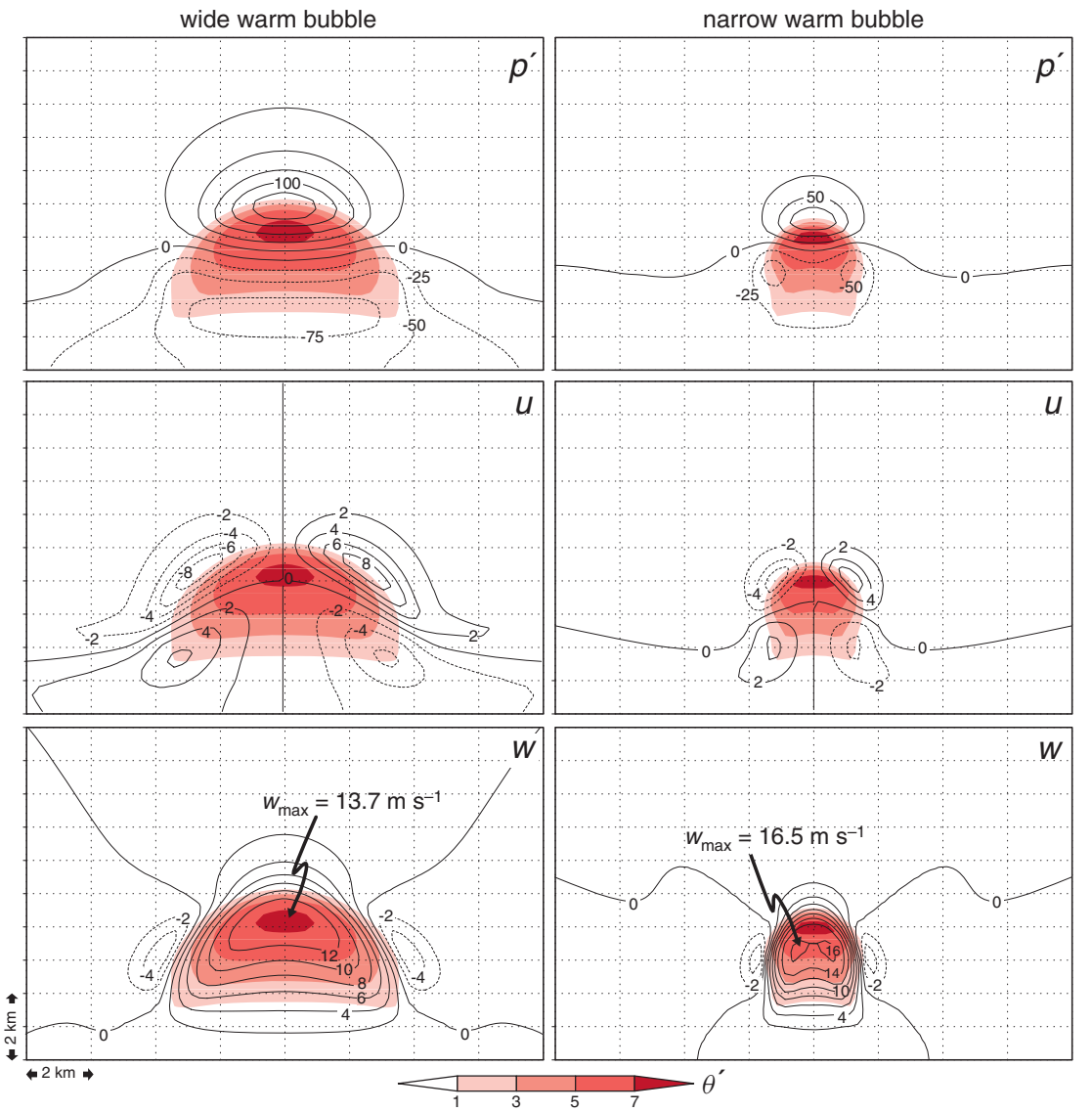

Figure 3.1 A comparison of the perturbation pressure (p') fields and zonal (u) and vertical (w) velocity components for the case of a wide warm bubble (left panels) and a narrow warm bubble (right panels) released in a conditionally unstable atmosphere in a three-dimensional numerical simulation. The contour intervals for p' and the wind components are 25 Pa and 2 m s^{-1}, respectively (dashed contours are used for negative values). Potential temperature perturbations (θ') are shown in each panel (refer to the color scale). The horizontal and vertical grid spacing is 200 m (the domain shown above is much smaller than the actual model domain). Both warm bubbles had an initial potential temperature perturbation of 2 K and a vertical radius of 1.5 km, and were released 1.5 km above the ground. The wide (narrow) bubble had a horizontal radius of 10 km (3 km). In the simulation of the wide (narrow) bubble, the fields are shown 800 s (480 s) after its release. The fields are shown at times when the maximum buoyancies are comparable. Despite the comparable buoyancies, the narrow updraft is 20% stronger owing to the weaker adverse vertical pressure gradient.

Because of the aforementioned effects of the vertical perturbation pressure gradient and entrainment, the development and intensity of convection are sensitive to updraft width. This sensitivity is not reflected in the stability analysis or estimate of maximum updraft speed provided by (3.7) and (3.16), respectively. The magnitude of pressure perturbations and the vertical perturbation pressure gradient increases as the width of the displaced parcel increases, whereas the detrimental effects of entrainment decrease as updraft width increases. Convection therefore favors up- and downdrafts having an intermediate width scale that is large enough to survive the dilution of buoyancy by mixing yet narrow enough that the perturbation pressure gradient force is not too suppressive. In the absence of entrainment, infinitesimally narrow drafts are favored.

In addition to the effects of the vertical perturbation pressure gradient and entrainment, the parcel theory prediction of the vertical acceleration of an air parcel and maximum updraft speed also neglects contributions to buoyancy from the presence of hydrometeors. In deriving (3.7), it was assumed that only temperature perturbations contributed to buoyancy. In deriving (3.17), although it was not indicated whether or not buoyancy included the effects of hydrometeor loading, buoyancy is virtually always expressed as the temperature or virtual temperature excess of an updraft parcel compared with its environment in the calculation of CAPE [recall (2.148) in Section 2.6], rather than by attempting to account for the condensate acquired within a rising updraft parcel via an expression for buoyancy like that given by (2.79) (large concentrations of hydrometeors can easily contribute the equivalent of a few degrees Celsius of negative buoyancy). In other words, CAPE usually is computed by assuming pseudoadiabatic ascent, such that hydrometeors are assumed to instantly fall out of a rising, saturated parcel such that the condensate mass does not affect the buoyancy. In contrast, in reversible moist adiabatic ascent, all condensate remains within the parcel (recall Figure 2.1). The condensate mass reduces buoyancy, but the condensate also carries heat (these two competing influences usually lead to a net reduction of buoyancy in the lower troposphere and a net increase in buoyancy by the time a lifted parcel reaches the upper troposphere).

Pseudoadiabatic and reversible moist adiabatic ascent are both idealized extremes; the influence of hydrometeors on the buoyancy realized by a real updraft lies somewhere in between. The buoyancy and the associated CAPE realized in pseudoadiabatic ascent are easier to compute than the buoyancy and CAPE assuming reversible moist adiabatic ascent, and are far easier to compute than the actual buoyancy and realized CAPE for a rising parcel. For this reason, CAPE calculations are usually based on the integrated temperature or virtual temperature excess based on pseudoadiabatic ascent (as in Section 2.6).

The freezing of water droplets within updrafts is an additional source of positive buoyancy above the melting level, although it is a much smaller source of buoyancy than condensational heating because the latent heat of fusion is only a small fraction of the latent heat of vaporization. The pseudoadiabatic lapse rate used to calculate CAPE does not consider freezing; thus, the neglect of freezing represents another limitation of parcel theory predictions of vertical velocity, albeit a relatively minor one.

Finally, compensating subsidence within the surrounding air, which can affect the buoyancy and/or the perturbation pressure field depending on how the base state is defined, was ignored in parcel theory, wherein the environment is assumed to be unchanged by the parcel.